ADVANCED MATERIALS

Supporting Information

for *Adv. Mater.*, DOI 10.1002/adma.202507013

Fundamental Limits on the Electron-Phonon Coupling and Superconducting T_c

Dmitrii V. Semenok, Boris L. Altshuler and Emil A. Yuzbashyan**

Supporting Information for "Fundamental limits on the electron-phonon coupling and superconducting T_c"

Dmitrii V. Semenok Boris L. Altshuler Emil A. Yuzbashyan**

Dmitrii V. Semenok
Center for High Pressure Science & Technology Advanced Research (HPSTAR), Bldg. 8E, ZPark, 10 Xibeiwang East Rd, Beijing, Haidian 100193, China
dmitrii.semenok@hpstar.ac.cn
Boris L. Altshuler
Physics Department, Columbia University, 538 West 120th Street, New York, NY 10027, USA
Emil A. Yuzbashyan
Department of Physics and Astronomy, Center for Materials Theory, Rutgers University, Piscataway, NJ 08854, USA
eyuzbash@physics.rutgers.edu

Contents

S1 Stability analysis

To evaluate the stability of a metal with respect to electron-phonon interactions, we use the standard kinetic equation for the electron distribution function $f(E,t)$[1, 2],

$$\left(1-\frac{\partial\Sigma}{\partial E}\right)\frac{\partial f}{\partial t}+\frac{\partial\Sigma}{\partial t}\frac{\partial f}{\partial E}=a_{\rm ep}I_{\rm ep}(E)+a_{\rm ee}I_{\rm ee}(E), \tag{S1}$$

where we added nonnegative constant coefficients $a_{\rm eph}$ and $a_{\rm ee}$ for convenience. The electron self-energy is

$$\Sigma=\fint dE'\int_0^\infty d\omega\,\alpha^2F(\omega)\frac{f(E'+\omega)-f(E'-\omega)}{E-E'}, \tag{S2}$$

and the electron-phonon collision integral is

$$I_{\rm ep}(E)=-2\pi\int_0^\infty d\omega\,\alpha^2F(\omega)\left\{N_0(T_{\rm ph})[2f-f_+-f_-]+f(f_+-f_-)+f-f_+\right\}, \tag{S3}$$

where $f\equiv f(E,t)$, $f_\pm\equiv f(E\pm\omega,t)$, and

$$N_0(T_{\rm ph})=\frac{1}{e^{\omega/T_{\rm ph}}-1} \tag{S4}$$

is the equilibrium Bose (phonon) distribution at temperature $T_{\rm ph}$. The kinetic equation (S1) assumes spatially uniform initial conditions and, as usual, that phonons remain in thermal equilibrium, see below and, e.g., [2], which also provides an explicit expression for the electron-electron collision integral $I_{\rm ee}$. We will prove that the metal is unstable when $C_{\rm el}<0$ by contradiction. Let

$$f(E,t=0)=f_0(T)\equiv\frac{1}{e^{E/T}+1} \tag{S5}$$

be the equilibrium Fermi distribution with temperature T that is slightly higher than the phonon temperature $T_{\rm ph}$. Experimentally, initial conditions of this type are created by heating the electrons with an ultrashort laser pulse[3, 4, 5]. Note, however, that we do not assume the two-temperature model, but merely chose an initial condition of the form (S5). The true fermion distribution $f(E,t)$ will generally become nonthermal in the course of the actual time evolution of the system.

Suppose the system is stable with respect to the electron-phonon interaction ($a_{\rm ep}=1$, $a_{\rm ee}=0$). Since the phonon specific heat is much larger than that of the electrons, $C_{\rm ph}/|C_{\rm el}|\sim E_F/\omega_D\gg1$, the change in the phonon temperature and, more generally, the deviation of the phonon distribution from the equilibrium Bose distribution $N_0(T_{\rm ph})$ is negligible. Phonons serve as a thermal bath for the electrons, and electrons equilibrate at temperature $T_{\rm ph}$ up to corrections of order ω_D/E_F, which are beyond the accuracy of the Eliashberg theory anyway.

Linearizing the kinetic equation and $f(E,t)$ around the equilibrium at $T=T_{\rm ph}$ with the help of the usual substitution[6],

$$f(E,t)=f_0+\delta f\equiv f_0(T_{\rm ph})+\frac{f_0(T_{\rm ph})\left[1-f_0(T_{\rm ph})\right]}{T_{\rm ph}}\varphi(E,t), \tag{S6}$$

we obtain after some algebra

$$\int dE'\,A(E,E')\dot\varphi(E',t)=-\int dE'\left[a_{\rm ep}M_{\rm ep}(E,E')+a_{\rm ee}M_{\rm ee}(E,E')\right]\varphi(E',t), \tag{S7}$$

where $A(E,E')$, $M_{\rm ep}(E,E')$, and $M_{\rm ee}(E,E')$ are *real symmetric* integration kernels (matrices) and $\dot\varphi\equiv\partial\varphi/\partial t$. Letting $\varphi(E,t)=e^{-\gamma t}\psi(E)$, we reduce the problem to a generalized eigenvalue equation of the form $\gamma A\psi=M\psi$. It is straightforward to show that $M_{\rm ep}$ and $M_{\rm ee}$ are positively defined for any electron-phonon couplings λ_i [by, e.g., considering the weak coupling limit where the system is obviously stable

($\gamma > 0$) for any physical phonon spectrum]. The assumption that the system is stable with respect to the electron-phonon interaction (i.e., for $M = M_{\rm ep}$) implies that A is positively defined as well. Since a linear combination of two positively defined real symmetric matrices with positive coefficients is similarly positively defined, it follows that it must also stable for $M = a_{\rm ep}M_{\rm ep} + a_{\rm ee}M_{\rm ep}$ for any $a_{\rm ep} > 0$ and $a_{\rm ee} > 0$.

Therefore, if the metal is stable with respect to the electron-phonon interaction, Equation (S1) must also be linearly stable for any choice of $a_{\rm ep} > 0$ and $a_{\rm ee} > 0$. Let $a_{\rm ee} \gg a_{\rm ep} > 0$. Then, electron-electron collisions dominate, and the electron distribution thermalizes essentially instantaneously with temperature $T(t)$, i.e., $f(E,t) = f_0(T(t))$, corresponding to the instantaneous energy density $\epsilon(t)$ of the electronic subsystem. However, since electron-electron collisions conserve $\epsilon(t)$ (this follows formally from $\int dEEI_{\rm ee}(E) = 0$), the latter is able to relax only through electron-phonon collisions. Multiplying Equation (S1) by E, integrating over E, and using $f(E,t) = f_0(T(t))$, we obtain

$$C_{\rm el}\frac{dT}{dt} = 2\pi\nu_0 a_{\rm ep}\int_0^\infty d\omega\alpha^2F(\omega)\omega^2\left[N_0(T_{\rm ph}) - N_0(T)\right], \tag{S8}$$

where

$$C_{\rm el} = 2\nu_0\int dEE\left\{\left(1 - \frac{\partial\Sigma_0}{\partial E}\right)\frac{\partial f_0}{\partial T} + \frac{\partial\Sigma_0}{\partial T}\frac{\partial f_0}{\partial E}\right\} \tag{S9}$$

is the electronic specific heat. Here Equation S9 and f_0 are the equilibrium electron self-energy and distribution function at temperature T. Equation (S9) for $C_{\rm el}$ was derived by Prange and Kadanoff in 1964[1] and later shown to be equivalent to Equation (1) in the main text[7, 8]. Note that there is a typo in [1] – the sign in front of $\frac{\partial\Sigma_0}{\partial E}$ should be minus and not plus as they have.

The right hand side of Equation (S8) is negative when $T > T_{\rm ph}$ indicating that the heat flows from hotter electrons to the colder phonon bath. Linearizing this equation in $(T - T_{\rm ph})$, we see that T grows exponentially when $C_{\rm el} < 0$. Note that Equation (S8) does not describe the actual dynamics of the system but is a consequence of the assumption that it is stable with respect to the electron-phonon interaction. Thus, $C_{\rm el} < 0$ is a *sufficient* condition of the instability. For further details on this stability analysis, see [9]. This reference also demonstrates that the loss of kinetic stability occurs at smaller values of λ, while $C_{\rm el}$ remains positive — that is, before the equilibrium Migdal-Eliashberg theory detects instability.

For $\lambda > \lambda_*$, the electronic specific heat is negative in a temperature interval from T_- to $T_+ > T_c$. In particular, $T_- \to 0$ and $T_+ \to 2.1335T_c$ in the strong coupling limit $\lambda \to \infty$[10]. However, a more complete kinetic analysis shows that the normal state remains unstable for all temperatures below T_- as well, emphasizing that $C_{\rm el} < 0$ is sufficient but not necessary for the instability. To put it another way, the normal state is unstable for all $T < T_+$ even though $C_{\rm el} < 0$ only for $T_- < T < T_+$. We also note that the existence of a new global minimum of the free energy just above T_c implies by continuity that the superconducting state is metastable at least for temperatures not too much below T_c[10].

S2 Proof of the stability condition $\xi < 1$

Since the primary theoretical result presented in this manuscript is the stability condition expressed by inequality (3) in the main text, we explicitly outline the logic underlying its derivation here rather than relying on previous publications.

ME theory is obtained from the stationary point of the action, describing electrons interacting through a retarded potential mediated by physical phonons. Provided the system is a stable metal, this stationary point corresponds to a global minimum of the thermodynamic potential[10]. Corrections to this stationary solution, known as loop corrections, are controlled by a small parameter—the ratio of the maximum phonon frequency to the Fermi energy[11, 12, 13, 14]. This fact, although presented differently, was originally demonstrated by Migdal and Eliashberg themselves[12, 13], who observed lattice instability at a bare coupling $\lambda_0 \approx 0.5$ within the Fröhlich Hamiltonian. They emphasized two essential conditions for their theory's validity: (1) a small ratio of maximum phonon frequency to Fermi energy, and (2) a sta-

ble lattice. This second condition has often been overlooked in subsequent studies employing effective electron-phonon models.

In typical metals, the ratio of the maximum phonon frequency to the Fermi energy ranges between 10^{-2} and 10^{-4}, thus providing excellent accuracy for evaluating the electronic specific heat. Indeed, it is well-established that the ME calculation of electronic specific heat consistently matches experimental results within a few percent accuracy[15, 16, 17, 18].

Our stability condition is proven by contradiction: assuming a stable metal described by a given Eliashberg function with Fermi energy much larger than the maximum phonon frequency, the ME formula for electronic specific heat, Equation 3 in the main text, must apply. However, the kinetic stability analysis of the previous subsection reveals instability when the specific heat becomes negative. Thus, a metal characterized by a negative ME electronic specific heat cannot physically exist, establishing inequality (3).

S3 Kinetic instability vs. polaronic and CDW instabilities arising from effective electron-phonon models

It is important to clearly distinguish the kinetic instability, which yields our stability condition, equation (3) in the main text, from the well-known polaronic/charge-density-wave (CDW)/lattice instabilities arising in effective electron-phonon models[11, 12, 13, 19, 20, 21, 22, 23, 24, 25, 26, 27, 28, 29, 30, 31, 32] (such as the Fröhlich or Holstein Hamiltonians). A key feature of our kinetic instability is that it establishes a strict upper bound on the *physical* electron-phonon interaction strength λ—a bound that, to the best of our knowledge, has not been previously identified. In contrast, polaronic/CDW transitions do not impose a sharp upper limit on λ, as $\lambda \to \infty$ at the onset of such instabilities[11, 12, 13, 20, 21, 33].

Secondly, while the polaronic/CDW/lattice instability describes an equilibrium phase transition, our kinetic instability is inherently a nonequilibrium phenomenon, occurring prior to any equilibrium phase formation. Moreover, the subsequent evolution following our instability does not necessarily lead to polaronic or CDW phases. For example, pressurized hydrides follow a completely different route, namely, hydrogen diffusion and the formation of new chemical compounds[39, 40, 41, 42, 43, 44].

Finally, the lattice instability observed in effective electron-phonon models is an artifact of these models, which at best, obscures the accompanying polaronic or CDW transitions. Fundamentally, the physical system is governed by the Coulomb Hamiltonian, describing electrons and ions interacting via Coulomb forces. Phonons naturally emerge as collective quasiparticle excitations from this Hamiltonian, inherently incorporating electron-ion interactions. Specifically, the electron density dynamically adjusts to ionic movements, leading to electronic polarization which directly shapes the phonon spectrum.

In simplified models such as the Holstein or Fröhlich Hamiltonians, the phonon frequency renormalization improperly counts the electronic polarization twice. This double-counting issue results in artificial phonon softening or lattice instability at a *bare* electron-phonon coupling $\lambda_0 \approx 0.5$. This spurious instability arises from incorrectly including the static part of the electron polarization operator more than once[34, 35], see also [27, 36, 37, 38]. Rigorous adiabatic perturbation theory starting from the Coulomb Hamiltonian does not produce such lattice instabilities[34, 35]. Hence, the instability seen in simplified electron-phonon models is essentially an artifact of double-counting (or "overscreening"[37, 38])—with ion-ion interactions effectively screened twice.

Indeed, Holstein, Fröhlich, and related models cannot be consistently derived from the underlying Coulomb Hamiltonian at any order of adiabatic perturbation theory[35], resulting in fundamental limitations. These effective models successfully capture phonon-mediated electron-electron interactions but fail to provide accurate phonon spectra. In reality, the Coulomb Hamiltonian naturally produces a unique phonon spectrum. Therefore, the standard and widely accepted practice in phonon-mediated superconductivity is to treat the phonon spectrum as an external input rather than attempting to renormalize it within these simplified effective models[15, 16, 45, 46].

Our approach avoids these pitfalls by directly working with physical phonons, employing the Eliashberg function as a fixed input. Rather than relying on effective electron-phonon models, our theory addresses

electrons interacting through retarded, phonon-mediated interactions. Consequently, a consistent formulation of our theory is inherently non-Hamiltonian, expressed instead via a nonlocal fermionic action, with the nonlocality reflecting the retarded nature of interactions mediated by physical phonons.

S4 Derivation of upper bounds on the electron-phonon interaction constant λ and T_c

It is helpful to disentangle the notions of the shape, height (overall scale), and support (spread) of the Eliashberg function $\alpha^2F(\omega)$ from each other. To this end, we introduce a normalized *shape* function

$$P(\omega) = \frac{1}{\lambda}\frac{2\alpha^2F(\omega)}{\omega}. \tag{S10}$$

By the definition of λ in Equation (4) in the main text and since $\alpha^2F(\omega) \geq 0$,

$$\int_0^\infty P(\omega)d\omega = 1, \quad P(\omega) \geq 0, \tag{S11}$$

so we can think of $P(\omega)$ as the distribution function of phonon frequencies. It determines the shape of the Eliashberg function, while λ controls its overall height. Note that we can specify λ and $P(\omega)$ independently of each other.

Now it is straightforward to determine the upper bound λ_* on the electron-phonon coupling λ from the stability condition [Equation (3) in the main text],

$$\lambda_* = \frac{1}{\max_T \left\{\int_0^\infty g\left(\frac{\omega}{2\pi T}\right) P(\omega)d\omega\right\}}. \tag{S12}$$

The function $g(x)$ reaches its single maximum $g_{\max} = 0.2709$ at $x_{\max} = 0.3273$. The upper bound λ_* is smallest, $\lambda_* = 1/g_{\max} = 3.6915$, for Einstein phonons, i.e., for $P(\omega) = \delta(\omega - \omega_E)$, because in this case the denominator of Equation (S12) assumes its maximum possible value $g_{\max}$. Similarly, Equation (S12) provides λ_* for other phonon spectra, e.g., for the Debye model [$P(\omega) = 2\omega/\omega_D^2$ for $\omega < \omega_D$ and zero otherwise] or for the same spectrum [same $P(\omega)$] as that for any of the materials in Extended Data Table S1. Furthermore, the definition of the stability parameter ξ in Equation (3) in the main text together with Equation (S12) imply Equation (5) in the main text.

To bound T_c, we need to bound both λ and the phonon spectrum. Suppose the highest phonon frequency is $\omega_{\max}$ and let $x = \omega/\omega_{\max}$. Then,

$$\lambda\langle\omega^2\rangle = \omega_{\max}^2 \frac{\int_0^1 x^2 P(x)dx}{\max_\tau \left\{\int_0^1 g\left(\frac{x}{\tau}\right) P(x)dx\right\}}. \tag{S13}$$

By analyzing the variational derivative of the right hand side of this equation with respect to $P(x)$, we find that it is maximal for $P(x) = \delta(x-1)$, i.e., for Einstein phonons with frequency $\omega_E = \omega_{\max}$. Taking this into account, we immediately obtain Equation (7) from Equation (6) in the main text.

S5 Properties and evolution of superconducting materials

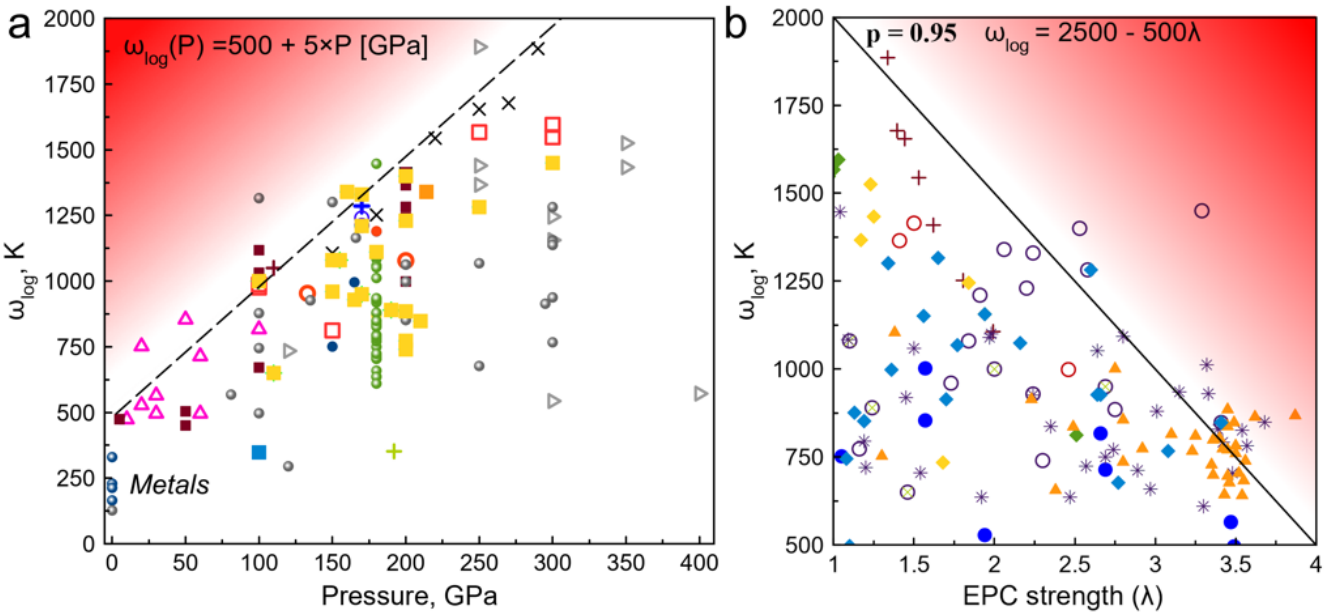

Figure S1: Statistical analysis of the results of DFT calculations of electron-phonon interaction parameters in metals, polyhydrides, and other compounds. (a) Correlation between the logarithmic average phonon frequency $\omega_{\log}$ in Kelvin and pressure P in GPa. For about 95% of the compounds $\omega_{\log}$ lies below the line $500 + 5P$. (b) Correlation between $\omega_{\log}$ in Kelvin and the electron-phonon coupling parameter λ. For about 95% of the compounds $\omega_{\log}$ in Kelvin falls below the line $2500 - 500\lambda$. Red areas indicate unlikely combinations of $\omega_{\log}$, P and λ. Data for the plot are from Refs. [53, 47, 49, 50, 51, 52, 48, 54].

Table S1: Various superconducting metals, compounds, and compressed polyhydrides and the values of T_c, electron-phonon coupling constant λ, stability parameter ξ, and average logarithmic ($\omega_{\log}$) and maximum ($\omega_{\max}$) phonon frequencies for them.

Compound	T_c, **K**	λ	ξ	$\omega_{\log}$, **K**	$\omega_{\max}$, **K**
		Experimental Materials			
Ga (amorph.)[55]	8.6	2.25	0.16	62	302
Pb (amorph.)[55]	7.2	1.91	0.29	35	155
Bi (amorph.)[55]	6.1	1.84 – 2.46	0.19	42	163
Hg[55]	4.2	1.0 – 1.6	0.14	86	165
Nb[55]	9.2	0.82 – 1.05	0.2	163	325
Nb_3Sn[56]	17.9	1.6 – 1.8	0.27	142	422
MgB_2[57]	40	0.87	0.16	680	1624
PbBi (amorph.)[58]	7.0	3.0	0.26	33.3	150
$PbBi_3$ (amorph.)[58]	6.8	2.78	0.23	33.4	154
H_3S (157 GPa)[41]	190	1.84	0.32	1078	2704
LaH_{10} (214 GPa)[59, 60]	245	2.06	0.43	1340	3145
YH_6 (165 GPa)[61]	224	1.71	0.39	1333	2450
ThH_9 (150 GPa)[62]	146	1.73	0.32	957	3362
ThH_{10} (170 GPa)[62, 63]	161	1.65	0.31	1116 – 1470	3122
YH_9 (205 GPa)[39, 53]	235	2.66	0.36	916 – 1054	3167
$(La,Y)H_{10}$ (180 GPa)[64]	253	3.87	0.47	868	3119
$(La,Ce)H_9$ (123 GPa)[43, 65]	190	2.27	0.33	582 – 915	2894
		DFT Calculations			
CaH_6 (172 GPa)[95]	215	2.69	0.42	950	2877
LaH_{16} (250 GPa)[67]	141	1.89	0.31	1511	3481
ScH_{12} (200 GPa)[68]	325	2.85	0.47	1189	2959
Li_2MgH_{16} (250 GPa)[69]	473	3.30	0.49	1111	3783
MgH_6[66]	263	3.29	0.58	1408	3719
Hydrogen ($I41/amd$, 500 GPa)[70]	374	2.85	0.45	1616	4089

Table S2: Data for Figure 1: evolution of superconducting materials in 20th – 21st centuries.

Material	**Year of discovery**	**Critical temperature, K**
Low-temperature superconductors[71]		
Hg	1911	4.2
Pb	1914	7.3
Nb	1933	9.7
NbN	1941	16
Nb_3Sn	1952	18.3
V_3Si	1953	17.1
Nb_3Ge	1973	23.2
NbTi	1962	9.2
CaC_6[72]	2005	11.5
MgB_2	2001	40
Unconventional superconductors[73]		
KWO_3	1967	6
$LiTi_2O_4$	1973	1.2
$BaPbBiO_3$	1975	13
La_2BaCuO_4	1986	30
$YBa_2Cu_3O_7$	1987	90
$BaKBiO_3$	1988	20
$BiSrCaCu_2O_6$	1988	105
$TlBa_2Ca_2Cu_3O_9$	1989	110
HgBa2CaCu2O6	1993	120
GdFeAsO	2008	53.5
SrFFeAs	2009	72
Superhydrides[71, 53]		
LaH_{10}	2018	250
ThH_9	2020	146
ThH_{10}	2020	161
YH_6	2021	224
YH_9	2021	243
CeH_9	2021	100
CeH_{10}	2021	115
BaH_{12}	2021	20
YH_4	2022	82
$(La,Y)H_{10}$	2021	253
Lu_4H_{23}	2023	70
SnH_4	2022	74
PH_3	2015	100
SbH_4	2023	115
$(La,Ce)H_{9-10}$	2023	190
NbH_3	2024	42

S6 Parameters of the electron-phonon interaction in various metals, alloys, and superhydrides

Table S3: Parameters of the electron-phonon interaction in metals, polyhydrides and, other compounds. We used this data to draw Figure 2.

Compound	Pressure, GPa	EPC strength (λ)	$\omega_{\log}$, K
DFT predictions			
ScH_9[47]	300	1.94	1156
VH_8[74, 75]	200	1.13	876
CrH_3[76]	81	0.95	568
ZrH_6[77, 78]	295	1.7	914
ZrH_{10}[79]	250	1.77	1068
NbH_4[80, 81]	300	0.82	938
SrH_6[49]	100	1.65	1316
HfH_{10}[79]	250	2.77	677
TaH_6[82]	300	1.56	1151
TiH_{14}[49, 83]	200	0.81	1063
Hf_3H_{13}[49]	100	1.1	497
RaH_{12}[49]	200	1.36	998
MgH_6[66]	300	3.29	1450
$CaYH_{12}$[84]	200	2.2	1230
$MgCaH_{12}$[85]	200	2.53	1400
YH_{10}[86, 87]	250	2.58	1282
ScH_{12}[88]	200	2.85	1189
Li_2MgH_{16}[69]	250	3.3	1111
ScH_4[47, 89]	250	0.81	1892
Metals and alloys (experiment)			
Nb[55]	0	1.05	229
V[55]	0	0.83	330
Sn[55]	0	0.72	165
Ta[55]	0	0.73	213
Hg[55]	0	1.3	86
a-Ga[55]	0	2.25	62
a-Pb*[55]	0	1.91	35
a-Bi[55]	0	2.46	42
Nb_3Sn[55]	0	1.7	142
MgB_2**[57]	0	0.87	680
a-PbBi[58]	0	3.0	33.3
a-$PbBi_3$[58]	0	2.78	33.4
Hydrides (experiment)			
$(La,Y)H_{10}$[64]	180	3.87	868
$(La,Ce)H_{9-10}$[43]	123	2.27	915
H_3S[90]	157	1.84	1080
LaH_{10}[91]	163	2.67	1118
YH_9[53]	200	2.75	885
YH_6[61]	170	2.24	1330
ThH_{10}[62]	170	1.91	1210
ThH_9[62]	150	1.73	960
YH_4[61]	155	1.1	1080
CeH_9[92]	110	1.46	650
CeH_{10}[93]	100	2.0	1000
SnH_4[94]	190	1.24	890
CaH_6[95]	170	2.69	950

*Amorphous film of Pb
**Given for comparison

Table S4: Values of the stability parameter ξ, electron-phonon coupling constant λ, and the average logarithmic frequency $\omega_{\log}$ for several hydrides at different pressures P.

Compound	P, GPa	ξ	λ	$\omega_{\log}$, K
CeH_9[92]	100	0.175	0.83	1421
	120	0.165	1.77	630
	150	0.152	0.86	1134
	200	0.131	0.69	1319
LaH_{10}[91]	∼50*	0.96	5.32	1031
	129	0.64	3.62	887
	163	0.53	2.67	1119
	214	0.43	2.06	1340
	264	0.37	1.73	1469
H_3S[90]	135	0.42	2.03	1482
	157	0.39	1.88	1579
ThH_{10}[63]	100	0.46	2.57	1048
	200	0.32	1.58	1184
	300	0.25	1.33	1150
CaH_6[95]	150**	0.58	2.97	964
	160	0.41	1.96	1204
	170	0.40	1.89	1419
	180	0.39	1.83	1249
	190	0.39	1.84	1333

*Extrapolation obtained by scaling the Eliashberg function at 129 GPa by a factor of 1.5. Extrapolated $T_c = 353$ K.
**DFT calculations for $P = 150$ GPa without accounting for the anharmonicity.

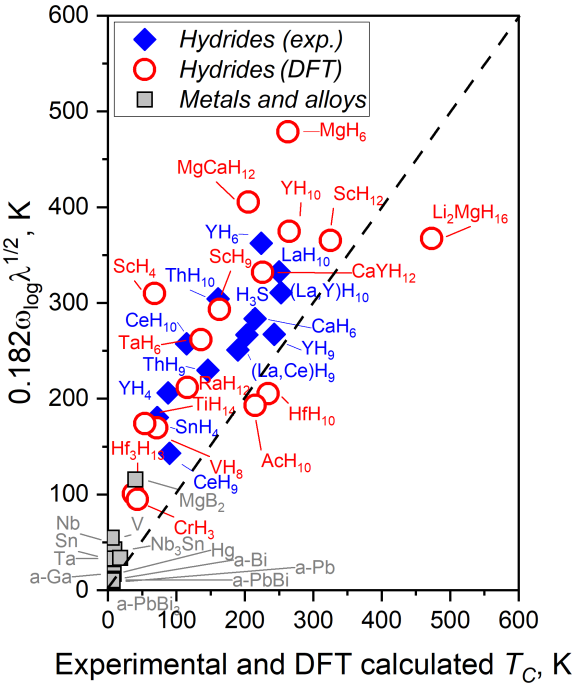

Figure S2: Comparison of experimentally observed and DFT calculated critical temperatures T_c for various superconductors with Allen-Dynes empirical strong coupling estimate $T_c^{\rm emp} = 0.182\omega_{\log}\sqrt{\lambda}$. Observe that for all experimentally studied hydrides $T_c < T_c^{\rm emp}$.

Table S5: Debye temperatures (T_D) for some superconducting metals, intermetallic compounds and compressed polyhydrides.

Compound	T_c, K	EPC parameter (λ)	T_D, K
Hg[55]	4.16	1.0 – 1.6	72
Nb[55]	9.22	0.82 – 1.05	277
Nb_3Sn[96]	17.9	1.6 -1.8	270
ThH_{10} (170 GPa)[62]	161	1.65	1350
YH_9 (205 GPa)[53, 39]	235	2.66	1275
$(La,Ce)H_9$ (123 GPa)[43, 44]	190	2.27	1107

References

[1] R. E. Prange and L. P. Kadanoff, Transport Theory for Electron-Phonon Interactions in Metals, Phys. Rev. **134**, A566 (1964).

[2] J. Rammer and H. Smith, Quantum field-theoretical methods in transport theory of metals, Rev. Mod. Phys. **58**, 323 (1986).

[3] J. Hohlfeld, S.-S. Wellershoff, J. Güdde, U. Conrad, V. Jähnke, E. Matthias, Electron and lattice dynamics following optical excitation of metals, Chem. Phys. **252**, 237 (2000).

[4] M. Lisowski, P.A. Loukakos, U. Bovensiepen, J. Stähler, C. Gahl and M. Wolf, Ultra-fast dynamics of electron thermalization, cooling and transport effects in Ru(001), Appl Phys A **78**, 165 (2004).

[5] B. Y. Mueller and B. Rethfeld, Relaxation dynamics in laser-excited metals under nonequilibrium conditions, Phys. Rev. B **87**, 035139 (2013).

[6] L. P. Pitaevskii and E.M. Lifshitz, Physical Kinetics: Volume 10 (Butterworth-Heinemann; 1st edition, 1981).

[7] W. Lee and D. Rainer, Comment on Eliashberg's free energy of a strong-coupling metal, Z. Physik B - Condensed Matter **73**, 149 (1988).

[8] S.V. Shulga, O.V. Dolgov and I.I. Mazin, Electron-phonon coupling and specific heat in $YBa_2Cu_3O_7$, Physica C **192**, 41 (1992).

[9] E. A. Yuzbashyan, B. L. Altshuler, A. Patra, Instability of metals with respect to strong electron-phonon interaction, Phys. Rev. Lett. (in press), arXiv:2409.19562 (2024).

[10] E. A. Yuzbashyan and B. L. Altshuler, Breakdown of the Migdal-Eliashberg theory and a theory of lattice-fermionic superfluidity, Phys. Rev. B **106**, 054518 (2022).

[11] A. A. Abrikosov, L. P. Gorkov, and I. E. Dzyaloshinski, *Methods of Quantum Field Theory in Statistical Physics* (Dover, New York, 1975).

[12] A. B. Migdal, Interaction between Electrons and Lattice Vibrations in a Normal Metal, Zh. Eksp. Teor. Fiz. **34**, 1438 (1958) [Sov. Phys.–JETP **7**, 996 (1958)].

[13] G. M. Eliashberg, Interactions between Electrons and Lattice Vibrations in a Superconductor, Zh. Eksp. Teor. Fiz. **38**, 966 (1960) [Sov. Phys.–JETP **11**, 696 (1960)].

[14] E. A. Yuzbashyan and B. L. Altshuler, Fluctuation corrections to the Eliashberg theory: The status of Migdal's theorem, unpublished.

[15] F. Marsiglio and J.P. Carbotte, *Electron-Phonon Superconductivity*, in K. H. Bennemann and J. B. Ketterson, (eds) Superconductivity. (Springer, Berlin, Heidelberg, 2008).

[16] J. P. Carbotte, Properties of boson-exchange superconductors, Rev. Mod. Phys. **62**, 1027 (1990).

[17] A. Subedi, L. Ortenzi, and L. Boeri, Electron-phonon superconductivity in APt_3P (A = Sr, Ca, La) compounds: From weak to strong coupling, Phys. Rev. B **87**, 144504 (2013).

[18] A. A. Golubov et al, Specific heat of MgB_2 in a one- and a two-band model from first-principles calculations, J. Phys.: Condens. Matter **14**, 1353 (2002).

[19] B.K. Chakraverty, Possibility of insulator to superconductor phase transition, J. Physique Lett., 40, 99 (1979).

[20] R. T. Scalettar, N. E. Bickers, and D. J. Scalapino, Competition of pairing and Peierls-charge-density-wave correlations in a two-dimensional electron-phonon model, Phys. Rev. B **40**, 197 (1989).

[21] F. Marsiglio, Pairing and charge-density-wave correlations in the Holstein model at half-filling, Phys. Rev. B **42**, 2416 (1990)

[22] V. V. Kabanov and O. Yu. Mashtakov, Electron localization with and without barrier formation, Phys. Rev. B **47**, 6060 (1993).

[23] P. Benedetti and R. Zeyher, Holstein model in infinite dimensions at half-filling, Phys. Rev. B **58**, 14320 (1998).

[24] Y. Ono and T. Hamano, Peierls Distortion in Two-Dimensional Tight-Binding Model, J. Phys. Soc. Jpn. **69**, 1769 (2000).

[25] A. S. Alexandrov, Breakdown of the Migdal-Eliashberg theory in the strong-coupling adiabatic regime, Europhys. Lett., **56**, 92 (2001).

[26] M. Capone and S. Ciuchi, Polaron Crossover and Bipolaronic Metal-Insulator Transition in the Half-Filled Holstein Model, Phys. Rev. Lett. 91, 186405 (2003).

[27] V. Z. Kresin and S. A. Wolf, *Colloquium:* Electron-lattice interaction and its impact on high T_c superconductivity, Rev. Mod. Phys. **81**, 481 (2009).

[28] I. Esterlis et. al., Breakdown of the Migdal-Eliashberg theory: A determinant quantum Monte Carlo study, Phys. Rev. B **97**, 140501(R) (2018).

[29] I. Esterlis, S. A. Kivelson, and D. J. Scalapino, Pseudogap crossover in the electron-phonon system, Phys. Rev. B **99**, 174516 (2019).

[30] B. Nosarzewski, E. W. Huang, Philip M. Dee, I. Esterlis, B. Moritz, S. A. Kivelson, S. Johnston, and T. P. Devereaux, Superconductivity, charge density waves, and bipolarons in the Holstein model, Phys. Rev. B **103**, 235156 (2021).

[31] O. Bradley, G. G. Batrouni, and R. T. Scalettar, Superconductivity and charge density wave order in the two-dimensional Holstein model, Phys. Rev. B **103**, 235104 (2021).

[32] C. Zhang, J. Sous, D. R. Reichman, M. Berciu, A. J. Millis, N. V. Prokof'ev, and B. V. Svistunov, Bipolaronic High-Temperature Superconductivity, Phys. Rev. X **13**, 011010 (2023).

[33] A. V. Chubukov, A. Abanov, I. Esterlis, S. A. Kivelson, Eliashberg theory of phonon-mediated superconductivity — When it is valid and how it breaks down, Ann. Phys., **417**, 168190, (2020).

[34] E.G. Brovman and Yu. Kagan, The phonon spectrum of metals, Zh. Eksp. Teor. Fiz. **52**, 557 (1967) [Sov. Phys.–JETP **25**, 365 (1967)].

[35] B. T. Gelikman, Adiabatic perturbation theory for metals and the problem of lattice stability, Usp. Fiz. Nauk **115**, 403 (1975) [Sov. Phys.–Usp. **18**, 190 (1975)].

[36] I. S. Tupitsyn, , A. S. Mishchenko, N. Nagaosa, and N. Prokof'ev, Coulomb and electron-phonon interactions in metals, Phys. Rev. B **94**, 155145 (2016).

[37] J. Berges, N. Girotto, T. Wehling, N. Marzari, and S. Poncé, Phonon Self-Energy Corrections: To Screen, or Not to Screen, Phys. Rev. X **13**, 041009 (2023).

[38] A. Marini, Equilibrium and out-of-equilibrium realistic phonon self-energy free from overscreening, Phys. Rev. B 107, 024305 (2023).

[39] P. Kong *et al.*, Superconductivity up to 243 K in the yttrium-hydrogen system under high pressure, Nat. Commun. **12**, 5075 (2021).

[40] W. Chen *et al.*, High-Temperature Superconducting Phases in Cerium Superhydride with a Tc up to 115 K below a Pressure of 1 Megabar, Phys. Rev. Lett. **127**, 117001 (2021).

[41] A. P. Drozdov, M. I. Eremets, I. A. Troyan, V. Ksenofontov and S. I. Shylin, Conventional superconductivity at 203 Kelvin at high pressures in the sulfur hydride system, Nature **525**, 73 (2015).

[42] V. S. Minkov, V. B. Prakapenka, E. Greenberg and M. I. Eremets, A Boosted Critical Temperature of 166 K in Superconducting D_3S Synthesized from Elemental Sulfur and Hydrogen, Angew. Chem., Int. Ed. **59**, 18970 (2020).

[43] W. Chen *et al.*, Enhancement of superconducting critical temperature realized in La-Ce-H system at moderate pressures, Nat. Commun. **14**, 2660 (2023).

[44] J. Bi *et al.*, Giant enhancement of superconducting critical temperature in substitutional alloy (La,Ce)H_9, Nat. Commun. **13**, 5952 (2022).

[45] P. B. Allen and B. Mitrovic, *Theory of superconducting* T_c, in Solid State Physics, edited by H. Ehrenreich, F. Seitz, and D. Turnbull (Academic, New York, 1982), Vol. 37, p. 1.

[46] M. V. Sadovskii, Limits of Eliashberg theory and bounds for superconducting transition temperature, Phys. Usp. 65 724 (2022).

[47] X. Ye, N. Zarifi, E. Zurek, R. Hoffmann and N. W. Ashcroft, High Hydrides of Scandium under Pressure: Potential Superconductors, J. Phys. Chem. C **122**, 6298 (2018).

[48] U. Pinsook, In search for near-room-temperature superconducting critical temperature of metal superhydrides under high pressure: A review, J. Met., Mater. Miner. **30**, 31 (2020).

[49] D. V. Semenok, I. A. Kruglov, I. A. Savkin, A. G. Kvashnin and A. R. Oganov, On Distribution of Superconductivity in Metal Hydrides, Curr. Opin. Solid State Mater. Sci. **24**, 100808 (2020).

[50] Y. Sun, S. Sun, X. Zhon and H. Liu, Prediction for high superconducting ternary hydrides below megabar pressure, J. Phys.: Condens. Matter **34**, 505404 (2022).

[51] P. Song, Z. Hou, K. Nakano, K. Hongo and R. Maezono, Potential high-T_c superconductivity in $YCeH_x$ and $LaCeH_x$ under pressure, Mat. Today Phys. **28**, 100873 (2022).

[52] M. G. Gebreyohannes, C. A. Geffe and P. Singh, Computational prediction of new stable superconducting magnesium hydrides at high-pressures, Phys. C **599**, 1354052 (2022).

[53] D. V. Semenok, Computational design of new superconducting materials and their targeted experimental synthesis, Doctoral program in materials science and engineering thesis, Skoltech (2022).

[54] P. Song, *et al.*, (La,Th)H_{10}: Potential High-T_c (242 K) Superconductors Stabilized Thermodynamically below 200 GPa, J. Phys. Chem. C **128**, 2656 (2024).

[55] P. B. Allen, Electron-phonon coupling constants, in Handbook of Superconductivity, edited by C. P. Poole, Jr. (Academic Press, San Diego, CA, 2000) Ch. 9, Sec. G, pp. 478-483.

[56] G. R. Stewart, Superconductivity in the A15 structure, Phys. C **514**, 28 (2015).

[57] Y. Kong, O. Dolgov, O. Jepsen and O. Andersen, Electron-phonon interaction in the normal and superconducting states of MgB_2, Phys. Rev. B **64**, 020501 (2001).

[58] T. T. Chen, J. D. Leslie and H. J. T. Smith, Electron tunneling study of amorphous Pb-Bi superconducting alloys, Physica **55**, 439 (1971).

[59] A. P. Drozdov *et al.*, Superconductivity at 250 K in lanthanum hydride under high pressures, Nature **569**, 528 (2019).

[60] M. Somayazulu *et al.*, Evidence for Superconductivity above 260 K in Lanthanum Superhydride at Megabar Pressures, Phys. Rev. Lett. **122**, 027001 (2019).

[61] I. A. Troyan *et al.*, Anomalous High-Temperature Superconductivity in YH_6, Adv. Mater. **33**, 2006832, (2021).

[62] D. V. Semenok *et al.*, Superconductivity at 161 K in thorium hydride ThH_{10}: Synthesis and properties, Mater. Today **33**, 36 (2020).

[63] A. G. Kvashnin, D. V. Semenok, I. A. Kruglov, I. A. Wrona and A. R. Oganov, High-Temperature Superconductivity in Th-H System at Pressure Conditions, ACS Appl. Mater. Interfaces **10**, 43809 (2018).

[64] D. V. Semenok *et al.*, Superconductivity at 253 K in lanthanum-yttrium ternary hydrides, Mater. Today **48**, 18 (2021).

[65] J. Bi *et al.*, Efficient route to achieve superconductivity improvement via substitutional La-Ce alloy superhydride at high pressure, arXiv:2204.04623 (2022).

[66] X. Feng, J. Zhang, G. Gao, H. Liu and H. Wang, Compressed Sodalite-like MgH_6 as a Potential High-temperature Superconductor, RSC Adv. **5**, 59292 (2015).

[67] I. A. Kruglov *et al.*, Superconductivity of LaH_{10} and LaH_{16} polyhydrides, Phys. Rev. B **101**, 024508 (2020).

[68] Q. Jianga *et al.*, Prediction of Room-Temperature Superconductivity in Quasi atomic H2-Type Hydrides at High Pressure, arXiv: 2302.02621 (2023).

[69] Y. Sun, J. Lv, Y. Xie, H. Liu and Y. Ma, Route to a Superconducting Phase above Room Temperature in Electron-Doped Hydride Compounds under High Pressure. Phys. Rev. Lett. **123**, 097001 (2019).

[70] D. Dangić, L. Monacelli, R. Bianco, F. Mauri and I. Errea, Large impact of phonon lineshapes on the superconductivity of solid hydrogen, Commun. Phys. **7**, 150 (2024).

[71] I. A. Troyan *et al.*, High-temperature superconductivity in hydrides, Phys. Usp. **65**, 748 (2022).

[72] T. E. Weller, M. Ellerby, S. S. Saxena, R. P. Smithand and N. T. Skipper, Superconductivity in the intercalated graphite compounds C_6Yb and C_6Ca, Nat. Phys. **1**, 39 (2005).

[73] A. M. Luiz, A simple model to estimate the optimal doping of p-Type oxide superconductors, Mater. Res-Ibero-Am J. **11** (2008).

[74] X. Li and F. Peng, Superconductivity of pressure-stabilized vanadium hydrides, Inorg. chem. **56**, 13759 (2017).

[75] E. Tikhonov, J. Feng, Y. Wang and Q. Feng, High-pressure stability and superconductivity of vanadium hydrides, Physica B: Condensed Matter **651**, 414603 (2023).

[76] S. Yu *et al.*, Pressure-driven formation and stabilization of superconductive chromium hydrides, Scientific reports **5**, 17764 (2015).

[77] K. Abe, High-pressure properties of dense metallic zirconium hydrides studied by ab initio calculations, Phys. Rev. B **98**, 134103 (2018).

[78] X.-F. Li, Z.-Y. Hu and B. Huang, Phase diagram and superconductivity of compressed zirconium hydrides, Phys. Chem. Phys. **19**, 3538 (2017).

[79] H. Xie *et al.*, Hydrogen Pentagraphenelike Structure Stabilized by Hafnium: A High-Temperature Conventional Superconductor, Phys. Rev. Lett. **125**, 217001 (2020).

[80] A. P. Durajski, Phonon-mediated superconductivity in compressed NbH_4 compound, Eur. Phys. J. B **87**, 1 (2014).

[81] G. Gao, G. *et al.*, Theoretical study of the ground-state structures and properties of niobium hydrides under pressure, Phys. Rev. B **88** (2013).

[82] Q. Zhuang *et al.*, Pressure-stabilized superconductive ionic tantalum hydrides, Inorg. Chem. **56**, 3901 (2017).

[83] J. Zhang, *et al.*, High-temperature superconductivity in the Ti-H system at high pressures, Phys. Rev. B **101**, 134108 (2020).

[84] X. Liang, *et al.*, Potential high-Tc superconductivity in $CaYH_{12}$ under pressure, Phys. Rev. B **99**, 100505 (2019).

[85] W. Sukmas, P. Tsuppayakorn-aek, U. Pinsook and T. Bovornratanaraks, Near-room-temperature superconductivity of Mg/Ca substituted metal hexahydride under pressure, J. Alloys Compd. **849**, 156434 (2020).

[86] C. Heil, S. Di Cataldo, G. B. Bachelet and L. Boeri, Superconductivity in sodalite-like yttrium hydride clathrates, Phys. Rev. B **99**, 220502(R) (2019).

[87] H. Liu, I. I. Naumov, R. Hoffmann, N. W. Ashcroft and R. J. Hemley, Potential high-Tc superconducting lanthanum and yttrium hydrides at high pressure, PNAS **114**, 5 (2017).

[88] Q. Jiang *et al.*, Prediction of Room-Temperature Superconductivity in Quasi atomic H_2-Type Hydrides at High Pressure, arXiv: 2302.02621 (2023).

[89] K. Abe, Hydrogen-rich scandium compounds at high pressures, Phys. Rev. B **96**, 144108 (2017).

[90] I. Errea *et al.*, Quantum hydrogen-bond symmetrization in the superconducting hydrogen sulfide system, Nature **532**, 81 (2016).

[91] I. Errea *et al.*, Quantum crystal structure in the 250-kelvin superconducting lanthanum hydride, Nature **578**, 66 (2020).

[92] W. Chen *et al.*, High-Temperature Superconducting Phases in Cerium Superhydride with a T_c up to 115 K below a Pressure of 1 Megabar, Phys. Rev. Lett. **127**, 117001, (2021).

[93] B. Li, *et al.*, Predicted high-temperature superconductivity in cerium hydrides at high pressures, J. Appl. Phys. **126**, 235901 (2019).

[94] I. A. Troyan *et al.*, Non-Fermi-Liquid Behavior of Superconducting SnH_4, Adv. Sci. **2303622**, 1 (2023).

[95] P. Hou, Z. Huo and D. Duan, Quantum and Anharmonic Effects in Superconducting Im-3m CaH_6 Under High Pressure: A First-Principles Study, J. Phys. Chem. C **127**, 23980 (2023).

[96] G. R. Stewart, Superconductivity in the A15 structure, Phys. C **514**, 28 (2015).